Proton Radiation Damage Assessment of a CCD for use in a Ultraviolet and Visible Spectrometer

J. P. D. Gow[a], J. Mason[a], M. Leese[a], B. Hathi[b], M. Patel[a,c]

[a], *School of Physical Sciences, The Open University, Walton Hall, Milton Keynes, MK7 6AA, UK*

[b], *Mullard Space Science Laboratory, University College London, Holmbury Hill Rd, Dorking, RH5 6NT, UK*

[c], *Space Science and Technology Department, Rutherford Appleton Laboratory, Harwell Campus, Didcot, QX11 0QX, UK*

E-mail: jason.gow@open.ac.uk

ABSTRACT: This paper describes the radiation environment and radiation damage analysis performed for the Nadir and Occultation for MArs Discovery (NOMAD) Ultraviolet and Visible Spectrometer (UVIS) channel launched onboard the ExoMars Trace Gas Orbiter (TGO) in 2016. The aim of the instrument is to map the temporal and spatial variation of trace gases such as ozone and dust/cloud aerosols in the atmosphere of Mars. The instrument consists of a set of two miniature telescope viewing optics which allow for selective input onto the optical bench, where an e2v technologies CCD30-11 will be used as the detector. A Geometry Description Markup Language model of the spacecraft and instrument box was created and through the use of ESA's SPace ENVironment Information System (SPENVIS) an estimate of the 10 MeV equivalent proton fluence was made at a number of radiation sensitive regions within NOMAD, including that of the CCD30-11 which is the focus of this paper. The end of life 10 MeV equivalent proton fluence at the charge coupled device was estimated to be 4.7×10^{9} protons.cm^{-2}; three devices were irradiated at different levels up a 10 MeV equivalent fluence of 9.4×10^{9} protons.cm^{-2}. The dark current, charge transfer inefficiency, charge storage, and cosmetic quality of the devices was investigated pre- and post-irradiation, determining that the devices will continue to provide excellent science throughout the mission.

KEYWORDS: Proton Damage, CCD, UVIS, NOMAD, ExoMars

Contents

1. Introduction

The ExoMars programme will investigate the Martian environment and demonstrate new technologies paving the way for future sample return missions [1]. The first mission consists of an Orbiter (Trace Gas Orbiter, TGO), on which the Nadir and Occultation for MArs Discovery (NOMAD) instrument is installed, and an entry, descent and landing demonstrator (Schiaparelli). NOMAD is a remote sensing instrument capable of measuring the spectrum of sunlight across a wide range of wavelengths including infrared, ultraviolet and visible. The Ultraviolet and Visible Spectrometer (UVIS) channel of NOMAD aims to map the temporal and spatial variation of trace gases such as ozone and dust/clouds in the atmosphere of Mars through remote sensing measurements [2]. The instrument consists of a set of two miniature telescope viewing optics which allow for selective input onto the optical bench, where an e2v technologies CCD30-11 will be used as the detector.

ExoMars TGO was launched in March 2016 and will spend 7 months travelling from the Earth to Mars, with Mars orbit insertion taking place in October 2016 after which it will spend around 6.2 years in orbit with the mission ending in February 2022. The science operation phase is expected to begin in December 2017 and last for 1 martian year (two Earth years), therefore it is important to understand the impact of the space radiation environment on the Charged Coupled Device (CCD) used in UVIS up to this point.

The main point of interest for this study was to investigate the space radiation environment the NOMAD instrument suite will experience, estimating the radiation exposure at key points within the instrument, and to predict the impact on the performance of the CCD used in UVIS and thus the impact upon the science performance of the overall instrument. The dark current and Charge Transfer Inefficiency (CTI) were investigated, and an analytical model created to

produce an image under the different UVIS operating modes as a function of radiation exposure and operational temperature to ensure data collection can be performed throughout the mission.

2. UVIS

The UVIS instrument has a dual telescope configuration; Nadir (downward viewing of the surface for total atmospheric column measurements) and solar occultation observations (SO, looking at the Sun through the atmosphere from orbit to measure vertical profiles). The telescopes are connected to a single spectrometer via a fibre optic link. Internally the spectrometer uses a UV coated back illuminated CCD 30-11 as its detector and a grating that gives UVIS with a spectral range of 200-650 nm at a resolution of ~ 1.5 nm. The combined instrument has a signal to noise ratio (SNR) of >500 in Nadir and >1000 in SO. An image of UVIS is shown in Figure 1.

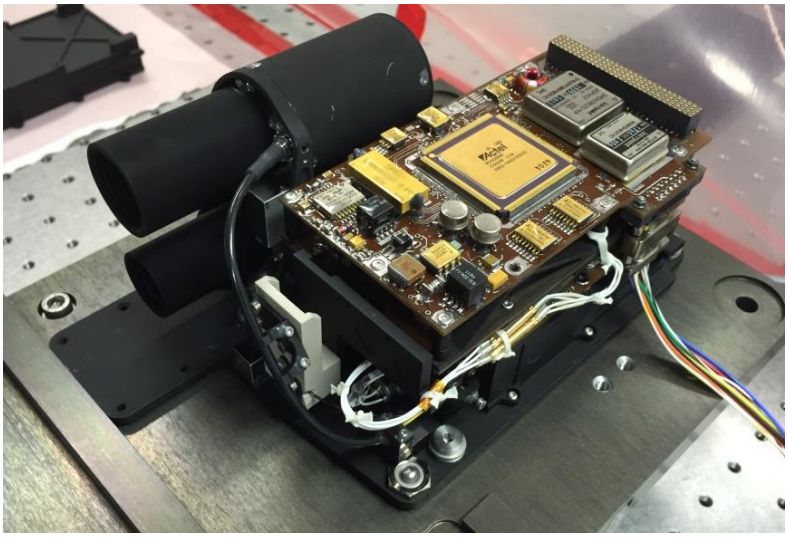

Figure 1: UVIS Flight Model instrument under test

UVIS can also be orientated by the spacecraft to perform limb observations or stellar occultation (similar to SO except viewing a stellar source). The temperature range experienced by UVIS, while in orbit around Mars, is expected to vary between -30° C and +20 °C, although the nominal operating temperature is expected to be 0 °C.

2.1 CCD30-11

The CCD30-11 is an Advanced Inverted Mode Operation (AIMO) Back Illuminated (BI) high performance three-phase buried channel CCD; details on the CCD are provided in Table 1 with further details available in the e2v data sheet [3]. The CCD to be used in UVIS was produced using e2v's Quantum Efficiency (QE) enhanced process with an ultraviolet coating applied to the CCD to increase the QE at short wavelengths. The addition of a boron implant under the integrating electrode defines a fixed potential well when the electrodes are all held at 0 V, which allows charge collection to be performed with the whole surface inverted minimising dark current generation and allowing the device to be operated at warmer temperatures. The devices

available for testing were from the same batch as the devices available for flight, and therefore should give comparable performance.

Table 1: CCD30-11 parameters based on pre- and post-irradiation measurements

Image area	26.6 x 6.7 mm
Active pixels (H)	1024
Active pixels (V)	255
Under-scan	8 pixels
Over-scan	8 pixels
Pixel size	26 x 26 µm
Readout Noise (correlated double sampling frequency 500 kHz)	9.3 e^- r.m.s.
Flight device full well capacity	430k e^-
Dark current generation pre-irradiation (20 °C, 0 °C and -30 °C)	466.1, 14.2, 0.3 $e^-.pixel^{-1}.s^{-1}$
Dark current generation mission end (20 °C, 0 °C and -30 °C)	13.9k, 1.66k, 54.4 $e^-.pixel^{-1}.s^{-1}$
Parallel Charge Transfer Inefficiency at 50k e^- pre-irradiation (20 °C, 0 °C and -30 °C)	2.8×10^{-6}, 8.4×10^{-7}, 6.3×10^{-7}
Parallel Charge Transfer Inefficiency at 50k e^- mission end (20 °C, 0 °C and -30 °C)	9.1×10^{-5}, 1.4×10^{-4}, 2.0×10^{-4}
Serial Charge Transfer Inefficiency at 50k e^- pre-irradiation (20 °C, 0 °C and -30 °C)	1.2×10^{-6}, 1.1×10^{-6}, 1.2×10^{-6}
Serial Charge Transfer Inefficiency at 50k e^- mission end (20 °C, 0 °C and -30 °C)	9.9×10^{-5}, 2.6×10^{-4}, 3.4×10^{-4}

3. Radiation Environment

The main exposure from the space radiation environment will arise from the transiting environment, i.e. cosmic rays, solar flares and solar proton events. The Earth's trapped environment will have a negligible contribution to the total end of life radiation exposure. Typically for space based semiconductor imagers the main source of damage from radiation is due to protons, because they are the most dominant charged particle in the space radiation environment.

ESAs SPace ENVironment Information System (SPENVIS) [4] was used to provide an estimation of the end of life proton fluence and ionising dose. The analysis performed used the Emission of Solar Protons (ESP) model, under solar maximum conditions, with the spacecraft held at 1 AU, as prescribed by the latest European Cooperation for Space Standardization [5]. Because of the nature of the solar cycle and the scheduled launch date the majority of the mission duration will take place at solar minimum. Cycle 24 also has the lowest recorded number of sunspots since cycle 14 in 1906 [6], therefore the actual dose received by a spacecraft

operating outside of the Earth's magnetic field is likely to be lower than predicted. To account for this a confidence value of 92% was used in SPENVIS to estimate the radiation environment.

The preliminary Computer-Aided Design (CAD) model of the spacecraft made available at the time of analysis, shown in Figure 2(a) [7]. The NOMAD instrument case and surrounding instruments were simplified to enable its adaptation into geometry description markup language format, shown in Figure 2(b), allowing it to be uploaded into the Sector Shielding Analysis Tool (SSAT) in SPENVIS. The dose at key points within NOMAD, including the location of the CCD, was then estimated for the time period up to the end of the science phase. The CCD end of life dose was estimated to be 1.9 krad with a 10 MeV equivalent proton fluence of 4.7×10^9 protons.cm^{-2}.

4. Experimental Arrangement and Technique

The CCD30-11 under test was mounted onto an aluminium cold finger attached to a two stage thermoelectric cooler with 1,000 Ω platinum resistance thermometers fitted to the device package and cold finger to monitor the temperature. Temperature control to ± 0.2 °C was provided by an ILX Lightwave controller (model number LDT-5525). An XTF5011/75-TH X-ray tube was used to fluoresce a polished manganese target held at 45° to the incident X-ray beam to provide a controllable number of 5,898 eV X-rays onto the CCD. Two Light Emitting Diodes (LED) were mounted facing the CCD to provide a diffuse optical background. Clocking and biasing were provided by an Xcam Ltd. USB2REM2 camera drive box in conjunction with drive software controlled use a custom MatLab software program.

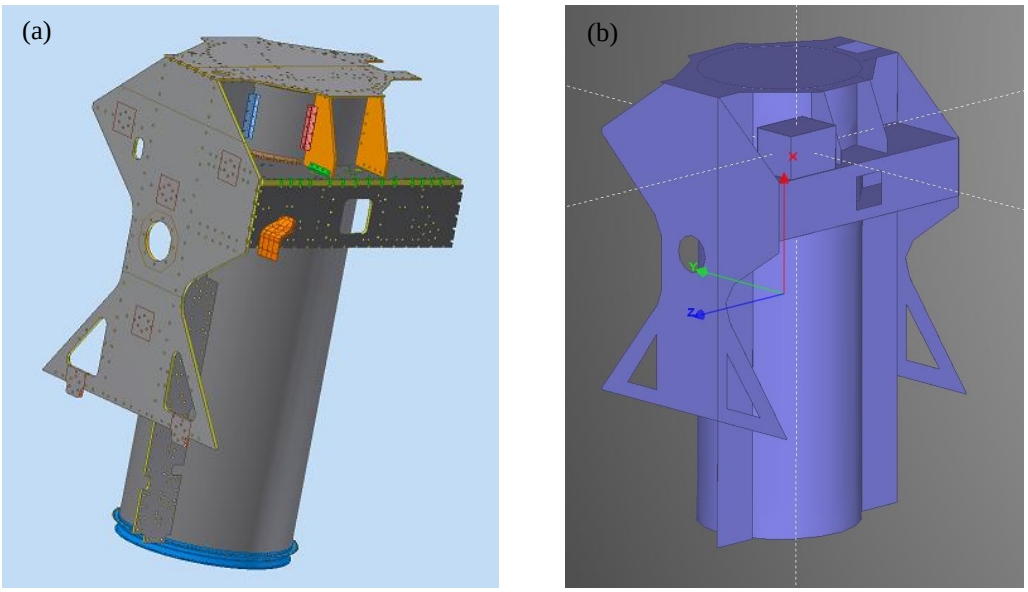

Figure 2: CAD and simplified representation of the ExoMars spacecraft, the central point is located at the central point of the NOMAD instrument

The device under test was operated using the potentials selected for inflight operation, and was read out using flight representative clocking. The process of clocking refers to the switching on and off of electrodes within the CCD pixel (parallel clocking) and register elements (serial clocking) to enable charge packets held under biased electrodes to be

transferred from one electrode to another. The charge packet is clocked through the image section towards the read-out register using the image clocks. One image clock cycle will cause one parallel transfer, with one row clocked into the read-out register. Before the next image clock cycle the register clocks are used to clock the charge packets towards the output circuit where the charge to voltage conversion takes place. Correlated Double Sampling (CDS) is used on the output signal to effectively remove reset, Johnson and flicker noise, whereby the signal voltage is determined by comparing the reference level (before charge is transferred into the output circuit) to the voltage level after charge is transferred into the output circuit. Further information on the operation of CCDs and CDS can be found in Janesick 2001 [8].

The register clock timings are shown in Figure 3 and the image clocks in Figure 4. To assess the device performance, data was collected between +20 °C to -30 °C; it is likely, however, that the CCD will spend the majority of its operational lifetime above 0 °C. The device characterisation included an assessment of the calibration, full well capacity, dark current and CTI using the Extended Pixel Edge Technique (EPER) [8].

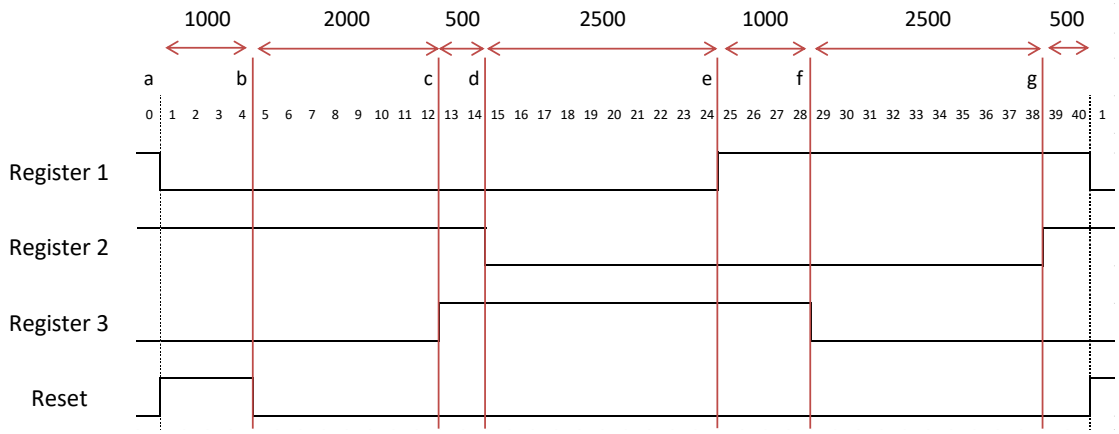

Figure 3: Register clock timings used to readout the device at 100 kHz, values are in ns

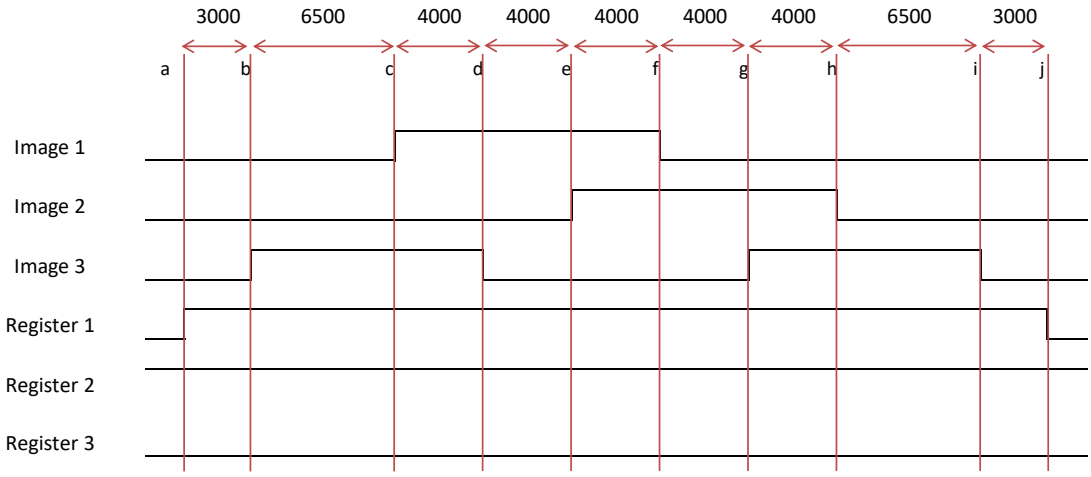

Figure 4: Image and register clock timings used to perform the parallel line transfer, values are in ns.

To provide an energy calibration, the noise peak location and the Mn-Kα peak location were found and assigned energy values of 0 eV and 5,898 eV respectively, providing an energy calibration in electrons per digital number or Analogue to Digital Conversion (ADC) number. The calibration was also measured using the Photon-Transfer Curve (PTC) technique [9], at 0 °C, where pairs of images were collected at multiple signal levels. The results from both techniques provide the same calibration value.

4.1 Dark Current

The dark current was measured using three images over a range of temperatures and the integration time was varied to avoid ADC saturation. During normal measurements the integration time used was between 30 and 160 s; during the substrate voltage (V_{ss}) characterisation the integration time was reduced to 10 s for V_{ss} below 7.5 V and 5 s for V_{ss} below 3.0 V.

4.2 Charge Transfer Inefficiency

The EPER measurement relies on taking a flat field exposure, and measuring the amount of deferred charge in the overscan to provide an estimation of the CTI. The CTI_{EPER} is given by [8]

$$CTI_{EPER} = \frac{S_D(e^-)}{S_{LC}(e^-)n_t} \quad (1)$$

where $S_D(e^-)$ is the average deferred charge, $S_{LC}(e^-)$ is the charge in the last column and n_t is the number of pixels transfers. CTI_{EPER} will not account for slow traps which release charge after a significant number of transfers (i.e. greater than the time to readout the selected number of overscan pixels) and the reported value is affected by the threshold used to determine what is deferred charge, for this study a fixed threshold of 20 electrons was used. The deferred charge was measured using 10,000, 25,000 and 50,000 electrons using optical light from two LEDs, with a uniformity of within 10 % across the device. Two images were collected to measure both serial CTI using an image size of 1640 columns and 260 rows and parallel CTI using an image size of 1040 columns and 856 rows. Separate images are collected to measure serial and parallel CTI independently to maintain the correct readout timings. Different regions of one device were irradiated to assess the impact of charge travelling through a number of un-irradiated pixels prior to the overscan region, this is discussed in more detail in Section 5.

To assess the impact of register clock overlap the period of overlap was decreased from the nominal 500 and 1000 ns to 70 and 140 ns, the overall readout speed remained at 100 kHz. The readout speed remained unchanged to minimise the impact on the flight electronics should a reduction in CTI be identified.

5. CCD Irradiation

The proton irradiation was performed using the Synergy Health Helios-3 Ion Beam to deliver 7.5 MeV protons to three CCDs. The levels used are given in Table 2. During the irradiation the devices were held inside a vacuum chamber connected onto the end of the beamline with the devices mounted in an unpopulated headboard with an aluminium shield to provide on-chip controls. The devices were irradiated as per Figure 5 which shows the regions irradiated. The flux rate is considerably higher than will be experienced in flight, however previous testing at room temperature using different fluxes with imaging sensors does not indicate an impact on

performance. Unless a flux of greater than $\times 10^{10}$ is used as this can thermally heat the silicon and damage the device. In the case of an irradiation performed at cryogenic temperatures the impact of flux on the stable defects present within the device as a function of time after the irradiation needs to be assessed as part of a future study. Based on the pixel size of this device and the flux used around 135 protons will interact within a pixel every second, therefore at a much lower temperature the defects created could interact with other nearby defects to form stable defects which, had the flux been lower have a lower probability of formation. The use of an alpha source to irradiate a CCD over an extended period of time while monitoring device performance, including the use of trap pumping [10 and 11] to monitor defect formation and evolution, would be ideal.

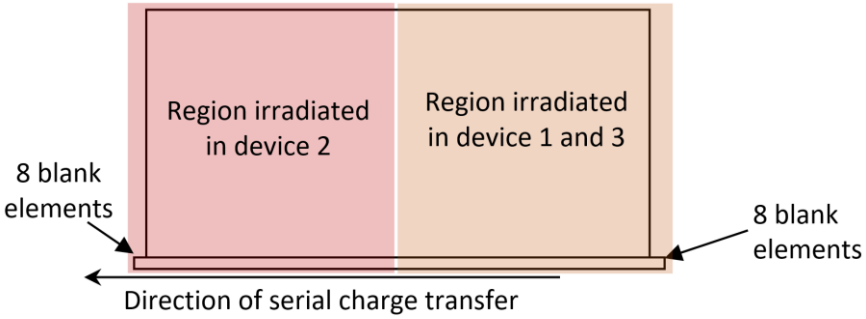

Figure 5: Diagram of the CCD30-11, highlighting the areas that were irradiated

Table 2: Irradiation details

Device	Image Area irradiated	Beam Energy (MeV)	Flux ($p.cm^{-2}.s^{-1}$)	Beam Fluence ($p.cm^{-2}$)	Equivalent fluence (10 MeV $p.cm^{-2}$)
1	50%	7.5	2.0×10^{7}	1.84×10^{9}	2.4×10^{9}
2	50%	7.5	2.0×10^{7}	3.60×10^{9}	4.8×10^{9}
3	50%	7.5	2.0×10^{7}	7.20×10^{9}	9.4×10^{9}
4	Control				

The irradiations were performed in quick succession at room temperature with the devices un-biased, the devices were at room temperature for three days after the irradiation prior to the start of data collection. Data collection per device took two days using automated test scripts, during this time the remaining devices were held at room temperature. The order in which the devices were tested post-irradiation was 3, 2, 1 and finally 4 (control). Previous tests with a Swept Charge Device (SCD) irradiated at room temperature and un-biased and tested over a similar temperature range, being held periodically at room temperature, did not indicate any measurable change in performance [12]. Therefore long term annealing, which is dependent on the temperature history of the device after irradiation will not have an impact on comparing device to device performance.

Ideally irradiations to assess the impact of radiation damage on imaging sensors for space applications should be performed at mission operating conditions, however this is not always practical. Particularly in the case of a mission where the temperature range is large, which could require irradiating multiple devices at different temperatures to provide the best indication of actual inflight performance. As part of another study a SCD was irradiated at -35.4 °C, and its performance at -35.4 °C monitored after the device had been held at room temperature for ever

increasing periods of time [13]. This study indicated that, when the device was clocked at 100 kHz, after being held at room temperature for a period of 24 hours the CTI increased from the post cryogenic irradiation value, this was then followed by a decrease with ever increasing time at room temperature. The dark current showed a continual decrease as the device was held at room temperature for increasing periods of time. With increasing times spent at room temperature the measured X-ray energy resolution moved towards the value measured in a SCD operated using the same conditions irradiated at room temperature.

It is difficult to predict the impact of annealing on the performance of the UVIS flight CCD, without having performed a cryogenic irradiation of a device from the same batch to assess the type and quantity of defects that are present and that could impact dark current generation and CTI. Considering the result from the SCD study and that the UVIS CCD will spend the majority of its operational lifetime above 0 °C, it is not expected that the annealing effects will be as great as in the SCD study. Therefore the worst case assumptions for the radiation environment that the CCD will be exposed to is expected to be sufficient to account for annealing effects during flight. Flight performance is monitored so this statement can be investigated during the course of the mission.

Larger devices with multiple image areas and output nodes allow different irradiations levels to be delivered to each image area. To avoid irradiating the adjacent image area a number of pixels on the edge of that image area are not irradiated, typically a gap of around 1 mm is left un-irradiated [14]. As EPER measurements rely on reaching an equilibrium of trapping and emission the concern is that by introducing a number of un-irradiated pixels on the edge of the device this could lead to an underestimation of the expected CTI_{EPER}. To investigate this concern the region irradiated in device 2 was flipped to investigate the impact on serial EPER measurements with an additional five hundred transfers through an un-irradiated region of the device. The impact was assessed by providing a linear fit to the data to assess any divergence in the result from device 2, with the parallel CTI measurements acting as the control indicating any non-linear relationship. Although not the primarily focus of the work discussed in this paper the initial results from this investigation have been included, these will be expanded on in a future publication which will include the use of a charge transport model.

6. Results and Discussion

The dark current was measured as a function of V_{ss} to enable the point at which the devices are no longer inverted to be readily identifiable, as would be expected there is a significantly larger increase in dark current at lower values of V_{ss} as the surface component is no longer suppressed. The point at which the device was no longer inverted was measured as 8.3 V, this value was taken as the point where the dark current was measured to have increased over the error on the measurement at 9.1 V. The flatband voltage shift for a CCD manufactured using the standard e2v process typically undergoes a voltage shift of between 0.1 and 0.2 V per krad. Therefore the flatband voltage shift experienced by the CCD30-11 used in UVIS will be around 0.4 V, or 0.8 V including a factor of two worst case. Therefore the minimum V_{ss} level for the UVIS instrument was recommended as 9.0 V.

The dark current was found to increase linearly with incident proton fluence. The dominant dark current generating trap post irradiation was identified using an Arrhenius plot of dark current against temperature, shown in Figure 6, where the exponential term is then given by:

$$-\frac{(E_g - E_t)}{k} \tag{2}$$

where E_g is the silicon bandgap, E_t is the trap level and $k = 8.62\times10^{-5}$ eV.K^{-1}. The dominant trap levels are 0.31 eV pre-irradiation, and around 0.43 eV post irradiation. These values compare well with previously measured trap levels of un-irradiated CCDs of 0.30 eV from an unknown defect [12 and 15] and post irradiation with other reported levels for the E-centre, 0.42 eV [15] and 0.44 eV [8 and 12].

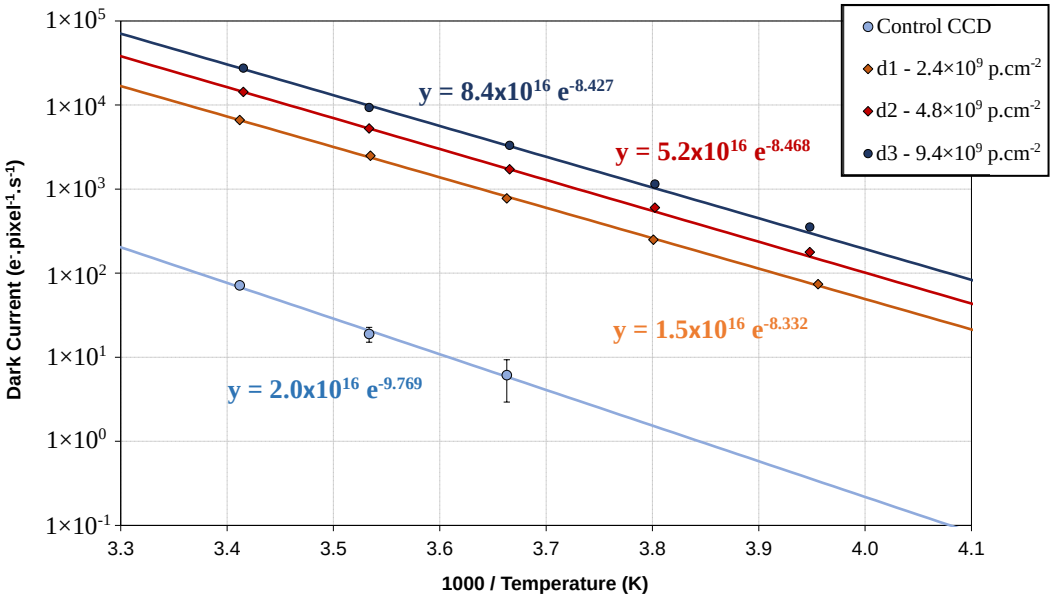

Figure 6: Dark current as a function of temperature and the exponential fits used to determine the dominant trap activation energy

An analytical model was created to allow a user to input the in-flight operational conditions, i.e. CCD temperature, proton fluence, UVIS operational mode and the image area of interest. This enabled the behavior of the detectors over the course of the mission to be assessed quickly and to visualize the impact of dark current increases on the images that will be produced. Considering the objectives of the UVIS instrument a conservative estimate of a dark current generation rate of 2000 e$^-$.pixel^{-1}.s^{-1} at 0 °C was made where above this level the scientific data generated using Nadir operation, integration time of 15 s will be compromised. During SO operation the integration time is only 100 ms, therefore the impact of dark current will be negligible until considerably higher generation levels. The dark current generation rate at 0 °C as a function of proton fluence is shown in Figure 7, the ideal threshold should only be exceeded after a 10 MeV equivalent proton fluence of 5.7×10^9 protons.cm^{-2}. A factor 1.2 times more than the predicted end of life, providing confidence that the CCD operation will not be prevented by increased dark current generation over the course of its operational lifetime.

The pre-irradiation CTI values were good for both parallel and serial transfers, i.e. $\times10^{-6}$ which is a typical CTI for an un-irradiated device, as would be expected lower signal levels had slightly elevated CTI. Post irradiation the CTI measured in the control regions was found to be comparable to the pre-irradiation values. The CTI measured for both parallel and serial transfers was found to decrease as a function of temperature, shown in Figure 8. The impact of the increasing CTI with decreasing temperature on the operation of the UVIS CCD will be countered by the reduction in dark current.

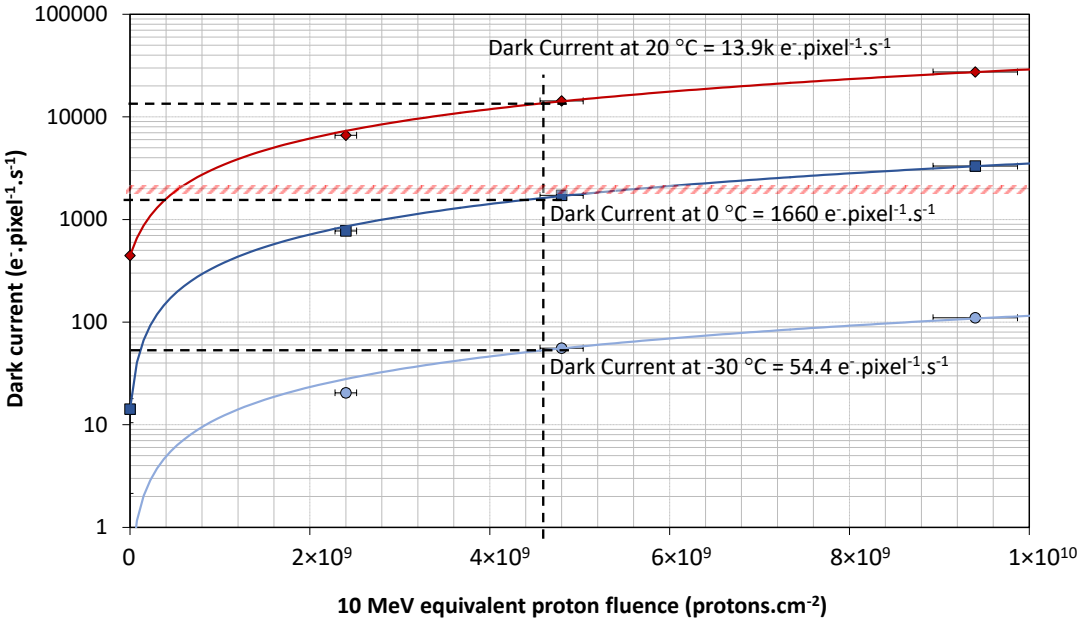

Figure 7: Dark current at 20°C, 0 °C and -30 °C as a function of proton fluence showing the desired dark current limit at 0 °C for the CCD operational lifetime at a factor 1.2 times that of the predicted end of life fluence

Considering the emission time constants of known n-channel trap species, E-centre, divacancy and A-centre [16], the parallel CTI would be expected to increase below -20 °C as the parallel dwell time approaches the E-centre emission time constant. The serial CTI would be expected to show no trend over the temperature range explored based on 100 kHz operation, with a slight increase in CTI at lower temperatures as the clock overlap of 500 ns approaches the divacancy emission time constant. The observed trends in Figure 8 instead show a decrease in CTI as the temperature is increased for both serial and parallel transfers. Therefore it is likely that the trend is dominated by the generation of dark current, which provides a temperature dependent background filling traps of between 50,000 electrons at 20 °C and 180 electrons at -30 °C in the device irradiated with 9.4×10^{9} protons.cm^{-2}. The presence of different levels of dark current makes relating the observed trends to trap emission time constants difficult, in particular in explaining the serial behaviour below 20 °C which shows a reduction. If an investigation of the traps impacting charge transfer was to be performed it would be important to keep the total amount of signal present within the CCD the same at all temperatures.

The serial and parallel CTI will be less than 5×10^{-4} towards the end of the CCDs operational lifetime at 0 °C at high signal levels. Due to the signal level the UVIS CCD will be handling, and that the majority of the operational lifetime will be spent above 0 °C where the CTI is shown to reduce, the impact of radiation induced charge transfer on mission operation should be minimal.

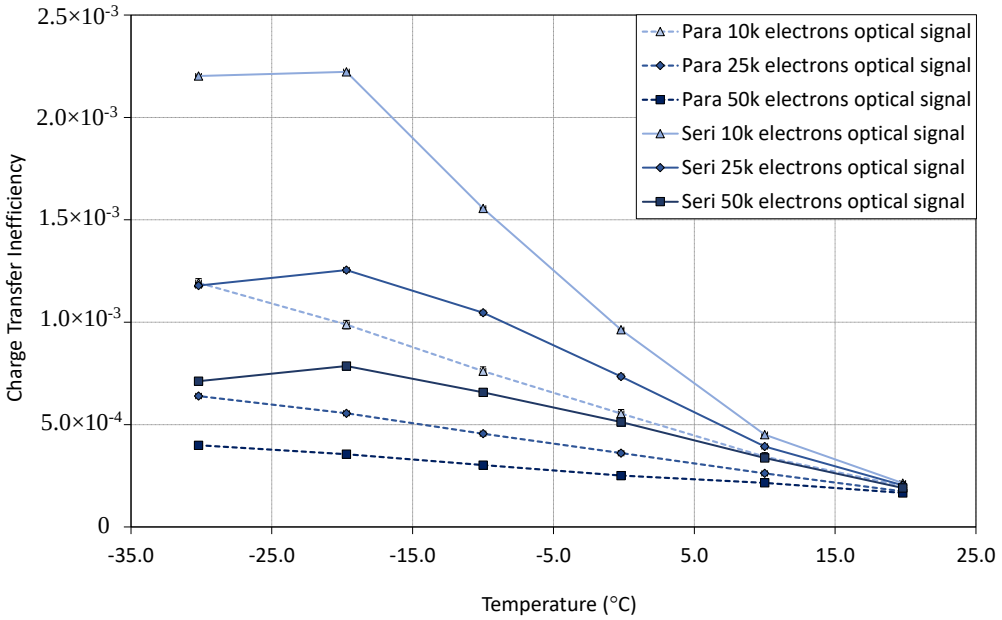

Figure 8: Parallel and serial CTI as a function of temperature measured in the CCD30-11 irradiated with a 10 MeV equivalent proton fluence of 9.4×10^{9} protons.cm^{-2}

As expected the relationship between CTI as a function of incident proton fluence is linear, the CTI measured at -30 °C, selected to provide minimal dark current to ensure comparable signal levels for each measurement, is shown in Figure 9. In the case of parallel CTI all measured data points are within error of a line of best fit, where the intercept was set at the mean pre-irradiation value for the three CCDs under test. In the case of the serial data collected at 4.8×10^{9} protons.cm^{-2} it is around 21 % lower than the line of best fit indicates, demonstrating a clear reduction in the reported value of CTI where a number of un-irradiated transfers take place before the edge of the device. Considering the behavior of different trap species, i.e. the emission and capture time constants, this impact could vary as a function of temperature, this will be investigated further in a later study. Assuming a linear relationship with the distance of un-irradiated silicon charge has moved through this could lead to an underestimation of 2 % to EPER measurements in a 12 μm pixel device, the CCD204 [14], with one hundred un-irradiated pixels.

After irradiation with 2.4×10^{9} protons.cm^{-2} no discernable trend could be identified in the results for serial CTI as a function of clock overlap, after 4.8×10^{9} a very slight trend could be identified and by 9.4×10^{9} protons.cm^{-2}, shown in Figure 10, a small trend can be observed between the different amounts of overlap. The cause of the small trend observed in Figure 10 is as a result of the relationship between the time trapped charge has to re-join the charge packet and the emission time constants of the different traps. The trap most likely responsible for the observed trend is the divacancy defect, as the shorter overlaps are comparable to its emission time constant at warmer temperatures and the longer overlaps comparable at the cooler temperatures explored. As the UVIS CCD will spend the majority of its operational lifetime above 0 °C and no discernable difference would be observed until well beyond the end of its operational lifetime, the current mode offers the best operating conditions.

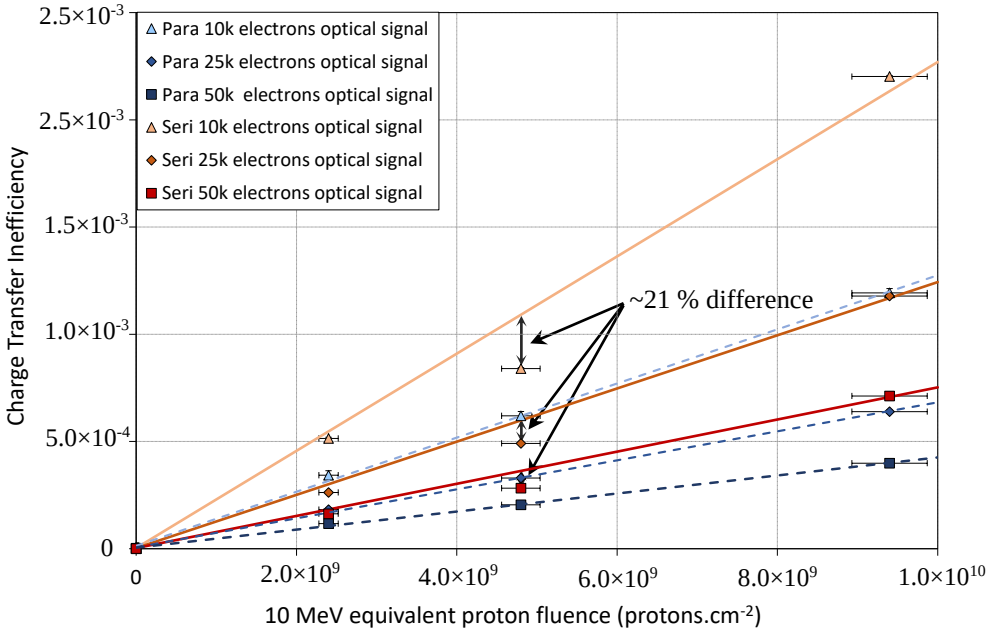

Figure 9: Parallel and serial CTI as a function of 10 MeV equivalent proton fluence showing the impact of 500 register transfers within an un-irradiated region to the device irradiated with 4.8×10^{9} protons.cm^{-2}

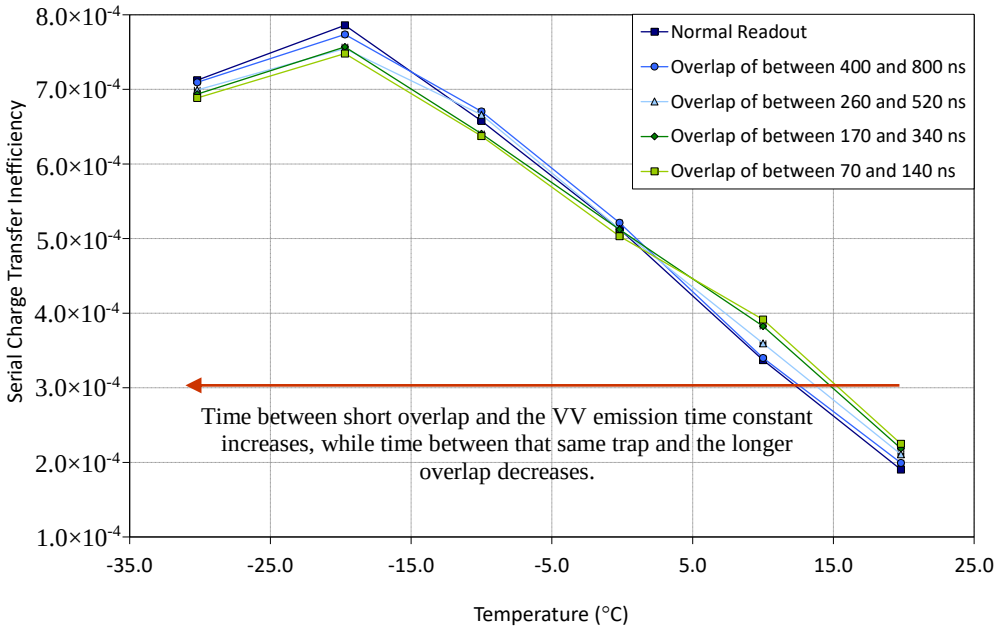

Figure 10: Serial CTI measured as a function of temperature using a transfer speed of 100 kHz with different clock width overlaps in the CCD30-11 irradiated with a 10 MeV equivalent proton fluence of 9.4×10^{9} protons.cm^{-2}

7. Conclusion

The assessment of the performance of UVIS flight comparable CCD30-11s over a range of proton fluence levels and the creation of an analytical model of CCD readout have demonstrated that the performance of the CCD used in UVIS, based on the radiation environment analysis described, should not be limited by radiation damage over its operational lifetime. UVIS will improve our understanding of martian ozone photochemistry (by global mapping and vertical profiling of ozone), characterise and map atmospheric aerosols (dust, ice), derive global UV climatology and investigate upper atmosphere airglow and other minor species (SNR permitting).

The dark current activation energies compare well with previously reported values, and the dark current limit of 2000 $e^{-}.pixel^{-1}.s^{-1}$, at 0 °C, will occur after a factor 1.2 times more than the predicted end of life. As the CCD will spend the majority of its operational lifetime above 0 °C and due to the amount of charge that will be incident on the device in-flight the impact of CTI on operational performance should be negligible.

The investigation into the impact of EPER CTI measurements performed where a number of un-irradiated pixels are traversed prior to the edge of the device indicated a factor of 21% underestimation in the measured CTI, when compared to a linear fit to the values where the edge of the device was irradiated. If the relationship is shown to be linear the impact on a CTI_{EPER} measurement with around one-hundred 12 μm un-irradiated pixels will be negligible. The subtleties of trap emission and capture will be explored further in a future study.

The observed trend in CTI using different register clock width overlaps raises an interesting point for consideration in future missions where there is a range of inflight operating temperatures. If there was a more significant change in CTI within the devices operational lifetime then the implementation of 'active clocking', i.e. where the clocking is altered subject to the operating temperature to ensure optimal CTI, could be considered.

Acknowledgments

The authors would like to thank Keith Jones of Synergy Health and Phillipa Smith of the Open University for their assistance with the irradiation.

References

[1] J. Vago, B. Gardini, G. Kminek, et al., *ExoMars - searching for life on the Red Planet*. 2006 ESA Bulletin (ISSN 0376-4265), No. 126, p. 16 – 23.

[2] M. R. Patel, et al., *The NOMAD Spectrometer on the ExoMars Trace Gas Orbiter Mission: Part 2 - Design, Manufacturing and Testing of the UVIS Channel*, *Applied Optics* (in preparation).

[3] e2v technologies, "CCD30–11 Back Illuminated High Performance CCD Sensor", 2006, A1A-100005 Issue 7.

[4] D. Heynderickx, B. Quaghebeur., E. Speelman and E. J. Daly, *Space environment information system (SPENVIS): A WWW interface to models of the space environment and its effects*, 2000 AIAA-2000-0371.

[5] ESA-ESTEC Requirements & Standards Division, *Space engineering, Space environment*, ECSS-E-ST-10-04C, 15th November 2008.

[6] Solar Cycle Prediction, Solar Physics, Marshall Space Flight Centre, last updated 1/8/13 https://solarscience.msfc.nasa.gov/predict.shtml

[7] TAS spacecraft CAD model

[8] J. R. Janesick, *Scientific Charge Coupled Devices*, SPIE Press Washington 2001.

[9] J. R. Janesick, *Photon Transfer*, SPIE Press Washington 2007.

[10] D. J. Hall, N. J. Murray, A. D. Holland, J. P. D. Gow, A. Clarke and D. Burt, *Determination of in situ trap properties in CCDs using a "single-trap pumping" technique*, 2014 IEEE Trans. on Nucl. Sci., vol. 61 no. 4.

[11] J. P. D. Gow, D. Wood, N. J. Murray, D. Burt, D. J. Hall, B. Dryer and A. D. Holland, *Post Irradiation Behaviour of a p-channel CCD Irradiated at 153 K*, 2016 Journal of Astronomical Telescopes, Instruments, and Systems, vol. 2 issue 2.

[12] J. P. D. Gow, *Radiation Damage Analysis of the Swept Charge Device for the C1XS Instrument*, PhD Thesis Brunel University 2009.

[13] J. P. D. Gow, P. H. Smith, P. Pool, D. J, Hall, A. D. Holland and N. J. Murray, *Proton Irradiation of a Swept Charge Device at Cryogenic Temperature and the Subsequent Annealing*, 2015 Journal of Instrumentation, 10(1), C01037.

[14] J. P. D. Gow, N. J. Murray, A. D. Holland and D. Burt, *Proton Damage Comparison of an e2v Technologies N-channel and P-channel CCD204*, 2014 IEEE Trans. Nucl. Sci. vol. 61 no. 4.

[15] A. D. Holland, *The effect of bulk traps in proton irradiated EEV CCDs*, 1993 Nucl. Inst. Meth. A, **vol. 326**, Issue 1-2.

[16] J. R. Srour, C. J. Marshall and R. W. Marshall, *Review of Displacement Damage Effects in Silicon Devices*, 2003 IEEE Trans. Nucl. Sci. vol. 50 no. 3.